Achieving Wireless Cable Testing for MIMO Terminals Based on Maximum RSRP Measurement

Zhang, Fengchun; Li, Mengting; Zhang, Xiang; Wang, Zhengpeng; Fan, Wei

Published in:
I E E E Transactions on Antennas and Propagation

DOI (link to publication from Publisher):
10.1109/TAP.2022.3162042

Publication date:
2022

Document Version
Accepted author manuscript, peer reviewed version

Achieving Wireless Cable Testing for MIMO Terminals Based on Maximum RSRP Measurement

Fengchun Zhang, Mengting Li, Xiang Zhang, Zhengpeng Wang and Wei Fan

***Abstract*—It is essential to perform end-to-end performance testing of multiple-input multiple-output (MIMO) systems under realistic propagation channel conditions. However, due to the highly integrated and compact radio frequency (RF) system design, the traditional conducted cable testing method is getting more and more problematic. The wireless cable solution, which can achieve the equivalent functionality of the conducted cable testing without actual RF coaxial cables, has attracted huge attention from industry and standardization for over-the-air (OTA) testing in recent years. However, the state-of-the-art solutions to achieve wireless cable testing necessitate at least reference signal received power (RSRP) reporting per device under test (DUT) antenna port for MIMO capable terminals, which is demanding and might not be accessible for commercial DUTs. In this work, a novel wireless cable solution based only on the maximum RSRP measurement of all DUT antenna ports is proposed, which can significantly alleviate the requirement of DUT RSRP reporting. To achieve the wireless cable testing, a novel calibration procedure is proposed to determine the transfer matrix between the probe antenna ports and the DUT antenna ports based on the DUT maximum reported RSRP measurement. The proposed algorithm is theoretically derived and experimentally validated for a 2×2 MIMO system, where an isolation above 25 dB is achieved for the measurement setup. The numerical simulation and experimental validation demonstrates the efficiency and robustness of the proposed algorithm.**

***Index Terms*—MIMO, spatial channel model, over-the-air testing, wireless cable method, RSRP reporting.**

I. Introduction

Conducted cable testing, i.e. testing performed while the antenna ports of the device under test (DUT) are connected to the testing instrument ports via radio frequency (RF) coaxial cables, has been the dominant solution in the industry for radio performance testing due to its simplicity and availability of accessible DUT antenna ports [1], [2]. Testing signals are directly routed to the respective DUT antenna ports undistorted, completely avoiding cross-talks and unwanted interferences to targeting antenna ports on the DUT. However, due to highly integrated system design in new radios, connectors to access DUT antenna ports have vanished and therefore DUT antenna ports become non-accessible for conducted testing purpose, which necessitates radiated over-the-air (OTA) testing [3]–[7]. In OTA testing, the DUT antennas are used as direct interfaces to receive/transmit the testing signals from probe antenna(s) that are connected to the testing instrument. Therefore, OTA radiated testing can eliminate the need for RF cable connections to DUT antenna ports. However, Due to the unguided nature of radio signal, the testing signals in an OTA setup will be distorted, which makes the OTA testing much more challenging compared to conventional cabled setups.

Several OTA methods have been investigated in the literature to address testing challenges for radio performance testing [2], [4], [8], [9]. The multi-probe anechoic chamber (MPAC) method aims to physically emulate the specified spatial channel models in the anechoic chamber, via controlling signals radiated from the multi-probe antennas connected to the radio channel emulator (CE). However, the MPAC solution might be too expensive, specially for 5G radios. The reverberation chamber (RC) solution aims to mimic rich multipath scenarios in the metallic enclosure with the help of mode stirrer. However, the RC solution might be difficult to emulate highly directive channel conditions. The wireless cable solution, which can achieve the conducted cable testing purpose yet avoiding the use of RF coaxial cables, has been an attractive solution for the industry and standardization. The basic idea is that the transfer matrix between the DUT antenna ports and probe antenna ports can be determined in the calibration stage and can then be calibrated out in the CE to ensure that testing signals are guided to respective antenna ports through the "wireless" cable connections, achieving the functionality of the conducted cable testing. Wireless cable solution has been widely applied for mobile terminal and automotive system testing, thanks to its unique features, e.g. low system cost, support for arbitrary spatial channel model implementation, and applicability for large DUTs [10]–[17].

The key to establish the wireless cable connection is to determine the transfer matrix. Several strategies have been proposed in the state-of-art works, as summarized below:

- The transfer matrix can be estimated, if known pilot sequences can be specified and communicated between the DUT and the testing instrument. Also, the estimated complex transfer matrix can be stored in the DUT and made accessible for testing purpose. This functionality, though promising, is generally not supported for current commercial mobile handsets [12].
- The transfer matrix can be directly calculated with the knowledge of the probe antenna patterns, free-space propagation coefficients between probe antennas and DUT antennas, and DUT antenna patterns. A non-intrusive, complex radiation-pattern measurement of DUT receive antenna patterns is described in [18], which requires Reference Signal Received Power (RSRP) measurement per

Fengchun Zhang, Mengting Li and Wei Fan are with the Antenna Propagation and Millimeter-wave Systems (APMS) section, Aalborg University, Denmark. Email: wfa@es.aau.dk

Xiang Zhang is with China Academy of Information and Telecommunications Technology (CAICT), Beijing 100191, China

Zhengpeng Wang is with Department of Electronics and Information Engineering, Beihang University, Beijing 100191, China

DUT antenna port as well as Reference Signal Antenna Relative Phase (RSARP) between antennas. While RSRP measurement per antenna port is standardized, RSARP measurement is not mandatory yet for commercial handsets. Furthermore, a large anechoic chamber is required to avoid multipath in the testing environment, which leads to high system cost [18]–[22].

- The transfer matrix can be designed to approximate an identity matrix directly, via employing polarization discrimination or antenna pattern discrimination scheme, as reported in [23] for some special DUTs. By doing so, there is no need to further calibrate the transfer matrix out. However, as explained in [23], this has specific and demanding requirement on the DUT antenna design (e.g. DUT antenna pattern and polarization), and thus it is not a generic solution.
- The transfer matrix can be estimated based on the RSRP measurement per DUT antenna port as explained in [15]–[17]. This solution has several unique advantages, e.g. it can be executed in a small RF shielded box and can support radio device with any multiple-input multiple-output (MIMO) order with a short calibration time.

For testing purpose, it is desirable that the testing can be done without the need for proprietary signal. That is, off-the-shelf commercial DUTs can be tested in their normal operational mode. Wireless cable solution has been successfully adopted by many major industrial players in recent years for 4G MIMO terminals where the RSRP value per DUT antenna port is available. However, according to the 3GPP document [24], commercial MIMO UE supporting 5G new radios will only need to report the maximal RSRP measurement among the RSRPs reported by the individual DUT ports. This largely reduced RSRP information of DUT ports will simplify the requirement for DUT RSRP reporting, yet posing great challenges in OTA testing for UE performance testing. As a result, current commercial software solutions are only capable of extracting maximum RSRP among DUT antenna ports for 5G handsets.

Due to this new limitation, the wireless cable solutions proposed in [15]–[17], which relies on RSRP measurement per DUT antenna port, would fail to work for 5G terminals. Hence, there is a strong need for a novel wireless cable solution to tackle this new limitation in the RSRP reporting. In this work, we aim to achieve wireless cable connections based on the maximal RSRP measurement, which has not been reported in the literature, to the best knowledge of the authors. With the proposed calibration procedure, the wireless cable connections can be achieved with minimal information extracted from the DUT (i.e. with only one maximum RSRP measurement), which can significantly alleviate the DUT RSRP reporting requirement and enable wireless cable testing for MIMO terminals supporting new radios.

The remainder of the paper is structured as follows. We firstly explain the signal model and the research question in Section II. Then, we discuss the proposed novel wireless cable solution based only on the maximum RSRP in Section III. After that, the measurement campaign to validate the proposed algorithm is described in Section IV. Finally, Section VI concludes the work.

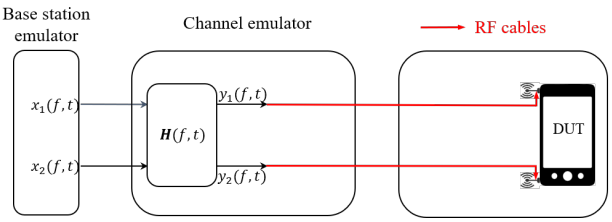

Figure 1. System diagram of conducted cable testing.

II. Problem Statement

Supposing a DUT equipped with N antenna ports serves as a receiver (RX), the target testing signal vector $\mathbf{y}(f,t) \in \mathbb{C}^{N\times 1}$ received at the DUT antenna ports, ignoring noise terms, can be expressed as:

$$\mathbf{y}(f,t) = \mathbf{H}(f,t)\mathbf{x}(f,t), \tag{1}$$

where $\mathbf{H}(f,t) \in \mathbb{C}^{N\times M}$ denotes the time-variant channel frequency response (CFR). Note that antenna radiation patterns for both the transmitter (TX) and the RX can be embedded in $\mathbf{H}(f,t)$ if known. $\mathbf{x}(f,t) \in \mathbb{C}^{M\times 1}$ is the signal vector transmitted by the M TX antenna ports. Performance testing aims to evaluate how the DUT would work when the specified signals $\mathbf{y}(f,t)$ are received at the respective DUT antenna ports.

In conducted testing as illustrated in Fig. 1, the specified testing signals are directly carried to the respective DUT antenna ports through RF cables. As explained in [15]–[17], wireless cable testing can achieve the equivalent functionality of conducted testing where the specified signals $\mathbf{y}(f,t)$ are guided to the respective antenna ports of the DUT via radio waves. This can be achieved via a pre-calibration scheme implemented in the CE as detailed below.

A 2×2 MIMO is taken as an example in the following discussion for simplicity, where the system diagram of wireless cable testing is illustrated in Fig. 2. Accordingly, the signal model can be written as:

$$\begin{aligned}\hat{\mathbf{y}}(f,t) &= \mathbf{A}\mathbf{A}^{inv}\cdot\mathbf{H}(f,t)\mathbf{x}(f,t)\\ &= \mathbf{A}\mathbf{A}^{inv}\cdot\mathbf{y}(f,t),\end{aligned} \tag{2}$$

where $\mathbf{A} \in \mathbb{C}^{N\times K}$ represents the transfer function matrix between the K CE output ports and the N DUT antenna ports, and $\mathbf{A}^{inv} \in \mathbb{C}^{N\times K}$ denotes the calibration matrix implemented in the CE. To mimic cabled testing functionality, $\mathbf{A}\mathbf{A}^{inv} = \mathbf{I}_N$, i.e. $\mathbf{A}^{inv} = \mathbf{A}^{-1}$ should be approximated, with $\mathbf{I}_N$ denoting a $N\times N$ identity matrix and $(\cdot)^{-1}$ indicating the inverse operator. Via implementing $\mathbf{A}^{inv}\mathbf{H}(f,t)$ in the CE, $\hat{\mathbf{y}}(f,t) = \mathbf{y}(f,t)$ can be accomplished in (2), i.e. wireless cable connections are established to carry the specified signals $\mathbf{y}(f,t)$ to the corresponding DUT antenna ports. Note that $K \geq N$, i.e. the number of the CE antenna ports no less than that of the DUT antenna ports, should be guaranteed so that $\mathbf{A}\mathbf{A}^{inv} \approx \mathbf{I}_N$ can be approximated in practice. As discussed, the inverse of the transfer function matrix $\mathbf{A}$, i.e. $\mathbf{A}^{inv}$, should be implemented in the CE to establish the desired wireless

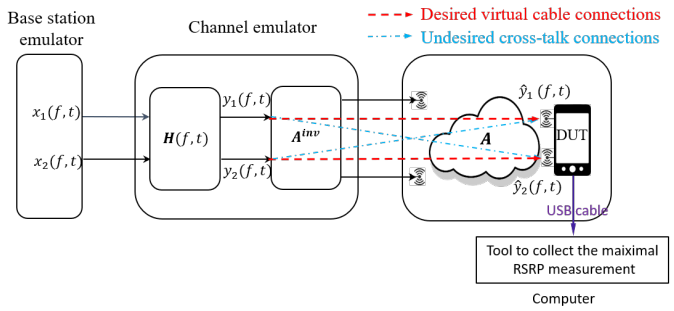

Figure 2. System diagram of wireless cable testing for a 2×2 MIMO.

cable connections. Thus, the main focus of this paper is on how to obtain the transfer function matrix $\mathbf{A}$.

Once the transfer function matrix $\mathbf{A}$ has been estimated, actual throughput measurements for specified channel models $\mathbf{H}(f,t)$ can thereby be conducted via implementing $\mathbf{H}(f,t)\mathbf{A}^{-1}$ in the CE. In the end, the performance of the DUT antenna can be evaluated under desired fading channel conditions.

It should be noted that the DUT antennas will be bypassed in the wireless cable and actual conducted cable setups. In the wireless cable concept, the transfer matrix $\mathbf{A}$ between the probe antenna ports and DUT antenna ports (which include the DUT antenna) will be determined and calibrated out via implementing $\mathbf{A}^{inv}$ in the CE, where the DUT antenna patterns are typically unknown. The quality of the achieved wireless cable is determined by the isolation between the achieved wireless cables, and the balanced power transmission in the wireless cable, while it is not relevant to the type of DUT antenna.

III. Proposed Solution

A novel wireless cable solution based on the maximum RSRP measurement is proposed in the paper. The system diagram is illustrated in Fig. 2, where the maximum RSRP reported by the DUT is collected by a computer through a universal serial bus (USB) cable.

A. Proposed Calibration procedure

As illustrated in Fig. 2, we can design a specific $\mathbf{A}^{inv}$ in the CE, and monitor the maximum RSRP reported by the DUT. In the calibration procedure, the objective is to properly design the $\mathbf{A}^{inv}$ in CE to ensure the matrix $\mathbf{A}$ can be accurately estimated based on the the maximum RSRP values reported by the DUT.

The proposed calibration procedure is described below:

1) Locate the DUT in an RF shielded box.
2) Set channel models in the bypassed mode via implementing $\mathbf{H}(f,t) = \mathbf{I}_2$ in the CE and $x_1(f,t) = x_2(f,t)$ in the base station(BS) emulator. By doing so, the effect of radio channel models is removed to simplify the calibration procedure.
3) Implement $\mathbf{A}^{inv} = \begin{bmatrix} 1 & 0 \\ e^{j\phi} & 0 \end{bmatrix}$ in the CE. Tune the phase ϕ from 0^o to 360^o and collect the maximal RSRP value for each phase state. The reported maximal RSRP can be denoted by $P_1(\phi)$, which can be calculated as:

$$\begin{aligned} P_1(\phi) &= \max\left\{ \left| \mathbf{A} \begin{bmatrix} 1 & 0 \\ e^{j\phi} & 0 \end{bmatrix} \mathbf{x}(f,t) \right|^2 \right\} \\ &= \max\left\{ \begin{bmatrix} P_1^1(\phi) \\ P_1^2(\phi) \end{bmatrix} \right\}, \end{aligned} \tag{3}$$

where the superscript n in $P_1^n(\phi)$ is used to denote the RSRP value at the n-th DUT antenna port. It can be observed from the above equation that the RSRP value at the n-th DUT antenna port $P_1^n(\phi)$ is only determined by the n-th row vector of matrix $\mathbf{A}$, and vise versa, meaning that the n-th row vector of matrix $\mathbf{A}$ can be estimated if and only if $P_1^n(\phi)$ is reported.

4) Implement $\mathbf{A}^{inv} = \begin{bmatrix} \alpha_1 & 0 \\ e^{j\phi} & 0 \end{bmatrix}$ ($\alpha_1 > 0$ and $\alpha_1 \neq 1$) in the CE. Set ϕ from 0^o to 360^o and collect the maximal RSRP value for each phase state. The reported maximal RSRP can be denoted by $P_2(\phi)$, which is given by:

$$\begin{aligned} P_2(\phi) &= \max\left\{ \left| \mathbf{A} \begin{bmatrix} \alpha_1 & 0 \\ e^{j\phi} & 0 \end{bmatrix} \mathbf{x}(f,t) \right|^2 \right\} \\ &= \max\left\{ \begin{bmatrix} P_2^1(\phi) \\ P_2^2(\phi) \end{bmatrix} \right\}. \end{aligned} \tag{4}$$

It is worth noting that a phase shift term introduced in either 1st or 2nd probe antenna port will only result in a circularly shift of the curve $P_1(\phi)$, which cannot introduce any extra RSRP measurements at DUT antenna ports needed for the calibration. In contrast, a real value α_1 is introduced to scale the signals transmitted by the 1st probe antenna, which might result in the discontinuous points (connecting RSRP curves in the 1st and 2nd DUT ports) in curve $P_2(\phi)$ located at different ϕ locations compared to those in curve $P_1(\phi)$. Thereby, some invisible segments of the RSRP curve of the 1st or 2nd DUT antenna ports in curve $P_1(\phi)$ might emerge in curve $P_2(\phi)$, introducing some extra RSRP measurements to help estimate the transfer matrix $\mathbf{A}$.

5) Implement $\mathbf{A}^{inv} = \begin{bmatrix} 1 & 0 \\ \alpha_2 e^{j\phi} & 0 \end{bmatrix}$ ($\alpha_2 \neq 1$ and $\alpha_2 \neq 1/\alpha_1$) in the CE. Set ϕ from 0^o to 360^o and collect the maximal RSRP value for each phase state. The reported maximal RSRP can be denoted by $P_3(\phi)$, which is written as:

$$\begin{aligned} P_3(\phi) &= \max\left\{ \left| \mathbf{A} \begin{bmatrix} 1 & 0 \\ \alpha_2 e^{j\phi} & 0 \end{bmatrix} \mathbf{x}(f,t) \right|^2 \right\} \\ &= \max\left\{ \begin{bmatrix} P_3^1(\phi) \\ P_3^2(\phi) \end{bmatrix} \right\}. \end{aligned} \tag{5}$$

Similarly, a real value α_2 is introduced here to scale the signals transmitted by the 2nd probe antenna, which might help provide more extra RSRP measurements in the estimation of matrix $\mathbf{A}$.

6) Check whether the RSRPs at both DUT antenna ports are visible in the power curves of $P_1(\phi)$, $P_2(\phi)$ and $P_3(\phi)$ to

ensure the transfer matrix $\mathbf{A}$ can be completely estimated. As discussed, the n-th row vector of matrix $\mathbf{A}$ is only determined by the RSRP values at the n-th DUT antenna port, i.e. $P_q^n(\phi)$ for $q \in [1, 3]$ according to equations in (3)-(5). Only one row vector of matrix $\mathbf{A}$ can be solved when the RSRP at only one DUT antenna port is visible in the power curves, i.e. when all of the 3 power curves are cosine curves without any discontinued points and their peak locations are aligned. In this case, the full $\mathbf{A}$ matrix cannot be determined and we need to generate a new solvable transfer matrix $\mathbf{A}$. This can be done by rotating either the DUT or the probe antennas and redo the above measurements to make sure that RSRPs at both DUT antenna ports are measured.

B. Numerical discussions

It has been proved in [15], [17] that if the RSRP power curves at both DUT antenna ports are reported for a 2×2, the matrix $\mathbf{A}$ is solvable when it is not rank deficient. For the new limitation in RSRP reporting, i.e. only the maximal RSRP among antenna ports is reported, if and only if the reported RSRP power curves are constructed by the RSRPs from both DUT antenna ports for a 2×2 MIMO system (indicating RSRPs at both DUT antenna ports are reported), matrix $\mathbf{A}$ will be solvable. When this pre-condition is met, the matrix $\mathbf{A}$ is solvable.

Below, some simulation examples are provided to explain how to check whether RSRPs at both DUT antenna ports are visible in the maximum RSPR curves and to illustrate how the scaling factors α_1 and α_2 introduce some extra RSRP measurements for matrix $\mathbf{A}$ estimation. In the simulation, the three power curves $\mathbf{P}_1$ (top sub-figure), $\mathbf{P}_2$ (middle sub-figure) and $\mathbf{P}_3$ (bottom sub-figure) are obtained according to (3)-(5) via setting the scaling factors $\alpha_1 = \alpha_2 = 0.5$. It should be noted that the RSRP curve at each DUT antenna port is a continuous cosine curve versus phase tuning ϕ, as illustrated by the blue dashed lines and the black dashed lines in Fig. 3, 4 and 5 corresponding to the RSRP curves for the 1st and the 2nd DUT port, respectively.

The RSRP curves of the 1st solvable matrix $\mathbf{A}$ example are plotted in Fig. 3. When the DUT only reports the maximal RSRP among the DUT ports, i.e. the larger RSRP at the 2 ports, for a given phase tuning state, the reported RSRP curves $\mathbf{P}_1$, $\mathbf{P}_2$ and $\mathbf{P}_3$ might be discontinuous curves, if they are constructed by the RSRP curve sectors at both DUT ports. As shown in the top sub-figure in Fig. 3, the $\mathbf{P}_1$ curve sector within $[49^o, 279^o]$ are the RSRPs reported by the 1st DUT antenna port while the rest two sectors are the RSRPs reported by the 2nd DUT antenna ports. The joint points (highlighted by the magenta ellipses) at 49^o and 279^o are the discontinuous points indicating that the RSRP reported is switched from one DUT antenna port to another. Similar discontinuous curves can be observed in the middle and bottom sub-figures in Fig. 3 as well. The power curves with discontinuous points indicate that RSRPs at both DUT antenna ports are included in the reported power curves, i.e. the precondition for a solvable matrix $\mathbf{A}$ is met. Comparing to the discontinues points in the top sub-figure, it can be seen that the locations of the discontinues points in the middle and bottom sub-figures are shifted due to the amplitude scaling factors, i.e. α_1 and α_2, implemented at the 1st and 2nd probe antenna, respectively. Therefore, the scaling factors can introduce some extra RSRP measurements for the estimation of matrix $\mathbf{A}$.

The RSRP curves of the 2nd solvable matrix $\mathbf{A}$ example are shown in Fig. 4. It can be seen in the top sub-figure that the maximum RSRP is a cosine curve without any discontinues point and overlaps completely with the RSRP of the 1st DUT antenna port, indicating that the RSRP of the 2nd DUT antenna port is invisible in this sub-figure, i.e. the 2nd row vector of the matrix $\mathbf{A}$ cannot be determined based on the measurement data in this sub-figure. Via attenuating the signals from the 1st probe antenna 6 dB, i.e. via setting $\alpha_1 = 0.5$, the maximum RSRPs reported by the DUT are plotted in the middle sub-figure. It shows that some RSRP measurements of the 2nd DUT antenna port become visible between the discontinues points (highlighted by the magenta ellipses), which are the extra RSRP measurements introduced by α_1. Hence, this $\mathbf{A}$ matrix is solvable as well due to visible RSRPs at both DUT antenna ports.

However, some matrices $\mathbf{A}$ are unsolvable due to RSRP measurements of one DUT antenna port is completely missing. The RSRP curves of an unsolvable matrix $\mathbf{A}$ example are shown in 5. It can be observed that all of the maximum RSRP curves in the sub-figures are cosine curves with aligned peak locations, demonstrating that RSRP at only one of the DUT antenna port is recorded, i.e. the RSRP at the 1st DUT antenna port. In this case, only the 1st row vector of matrix $\mathbf{A}$ can be determined as explained, while the 2nd row vector of matrix $\mathbf{A}$ cannot be determined due to the lack of RSRP at the 2nd DUT antenna port. A matrix $\mathbf{A}$ is typically unsolvable, when the relative phase between the entries in the 1st row vector is close to that in the second row vector or the amplitudes of the entries in one row vector are much larger than the other. As discussed, we need to generate a new $\mathbf{A}$ matrix and redo the calibration measurements in these cases.

Furthermore, some noises in a practical setup are unavoidable, for instance, the noises introduced by the phase shifters, attenuators and the noise in the measurement environment, which will cause some errors to the estimation of matrix $\mathbf{A}$. However, the noises will only introduce estimation errors in matrix $\mathbf{A}$ but it will not lead to unsolvable matrix $\mathbf{A}$. As discussed in reference [17], The calibration accuracy is strongly dependent on the property of matrix $\mathbf{A}$ and signal to noise ratio (SNR) at the DUT antenna ports, which are determined by the measurement configuration and surroundings.

The wireless cable solutions only work when the transfer matrix $\mathbf{A}$ is frequency flat over a system bandwidth of interest, since the RSRP values are the mean power over the frequency band (e.g. up to 20MHz for LTE system). The transfer matrix $\mathbf{A}$ in a reflective environment, e.g. a reverberation chamber, will result in a fluctuated matrix $\mathbf{A}$ over the frequency band. Thus, the wireless cable testing is typically conducted in an anechoic enclosure to meet the frequency flat assumption of the matrix $\mathbf{A}$. Moreover, the measurement configuration and surroundings will determine the condition number of the matrix $\mathbf{A}$. As explained in [17] a matrix $\mathbf{A}$ with a

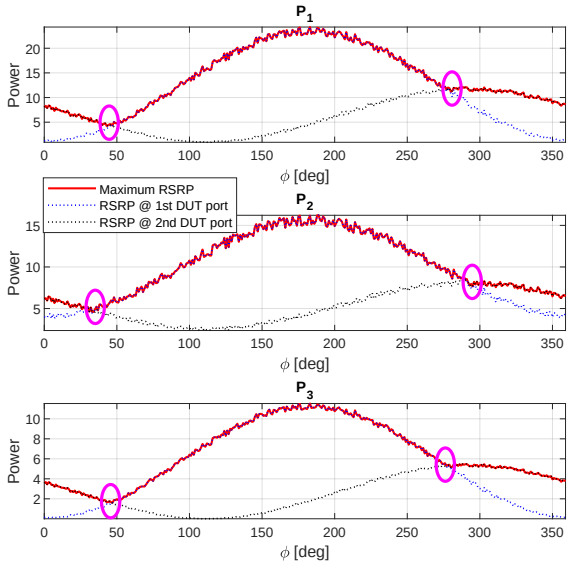

Figure 3. Power curves for the 1st solvable matrix $\mathbf{A}$ example.

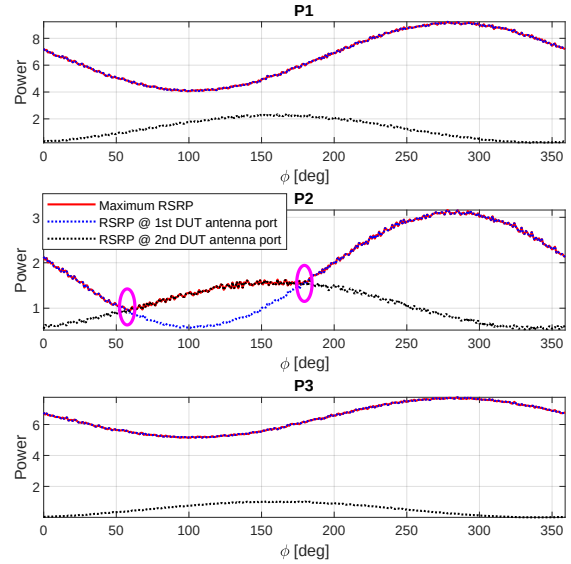

Figure 4. Power curves for the 2nd solvable matrix $\mathbf{A}$ example.

smaller condition number is desirable, since the estimation accuracy of the matrix $\mathbf{A}$ in (7) and the implement accuracy of $\mathbf{A}^{inv} = \mathbf{A}^{-1}$ will be less likely to be affected by the measurement noise and the uncertainties of phase shifters and attenuators. Therefore, the condition number of the matrix $\mathbf{A}$ has a significant impact on the wireless cable performance. In practice, the matrix $\mathbf{A}$ might be not solvable when it is rank deficient or not favorable due to its large condition number. There are several ways in practice to improve the condition of the matrix $\mathbf{A}$, as explained in [15], [17]. for instance, we can rotate the DUT to change the matrix $\mathbf{A}$. Or we can have more CE probes divided to several groups and measure the matrix $\mathbf{A}$ for each group. We can then select the group of the probes for the resulted matrix $\mathbf{A}$ with the lowest condition number.

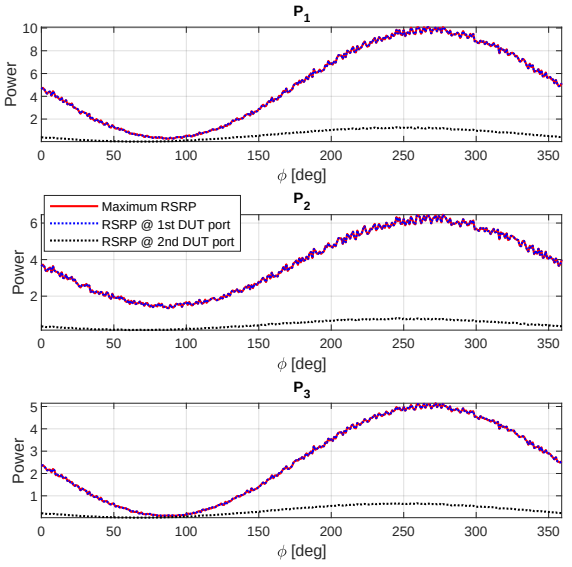

Figure 5. Power curves for an unsolvable matrix $\mathbf{A}$ example.

For a transfer matrix $\mathbf{A}$ with a given condition number, the lower noise (the higher SNR) received at DUT antenna ports, a more accurate estimation of matrix $\mathbf{A}$ can be achieved and thereby better wireless cable connections can be established. For explanation simplicity, the noises are not considered in the formulation and in the simulation. However, they are involved in the practical measurement. Noise is typically not a major problem in the wireless cable setup since the measurement is generally performed in a shielded anechoic box.

C. Partical swarm optimization (PSO) algorithm

Due to the non-linearity of the equations in (3)-(5), the transfer function matrix $\mathbf{A}$ cannot be directly solved using an inverse matrix approach. The estimated power vectors can be completely determined by the matrix $\mathbf{A}$ according to (3)-(5). Therefore, a data fitting method is applied to determine the matrix $\mathbf{A}$ via minimizing the distance between the estimated and the measured power vectors, which can be expressed by the objective function below:

$$\min_{\mathbf{A}} F(\mathbf{A}), \tag{6}$$

with the normalized distance function $F(\mathbf{A})$ defined by

$$F(\mathbf{A}) = \frac{\left\| [\mathbf{P}_1\ \mathbf{P}_2\ \mathbf{P}_3] - [\hat{\mathbf{P}}_1\ \hat{\mathbf{P}}_2\ \hat{\mathbf{P}}_3] \right\|}{\left\| [\mathbf{P}_1\ \mathbf{P}_2\ \mathbf{P}_3] \right\|}, \tag{7}$$

where $\|\cdot\|$ denotes the Frobenius norm of the matrix. $\mathbf{P}_q$ with $q \in [1, 3]$ is the measured power curves and $\hat{\mathbf{P}}_q$, with $q \in [1, 3]$ represent the estimated power curves, i.e. synthesized based on the estimated matrix $\mathbf{A}$.

To determine the 4 complex variables in the transfer function matrix $\mathbf{A}$, a brute-force searching method can be applied. However, an 8-dimensional brute-force searching might be infeasible in practice due to the extremely long searching time. Therefore, a faster and more efficient PSO algorithm is

proposed for the determination of the transfer function matrix $\mathbf{A}$, according to the objective function in (6), where the PSO algorithm is referred to [25]–[27].

As explained, 4 complex variables in the matrix $\mathbf{A}$, i.e. 4 parameters, need to be determined. For each parameter, an amplitude term within $[0, \alpha_{max}]$ and a phase term within $[0, 2\pi)$, are defined for the solution space, where $\alpha_{max} = \sqrt{\max\{\mathbf{P}_1\}}$ is used to bound the amplitude searching space.

In the PSO implementation, a population of 30 is set for the swarm, both correction factors c_1 and c_2 are set to 2, and the maximum number of iterations is set to 200.

As discussed in [17], [26], [28], the PSO algorithm might stagnate in a local optimization solution, meaning that it cannot always guarantee a global optimization solution to be found, though highly likely to. In order to increase the probabilities of finding the global optimization solution, 10 realizations are run and the best solution, i.e. the one with the minimum $F(\mathbf{A})$, is selected as the estimated matrix $\hat{\mathbf{A}}$.

IV. Measurement Validation

A preliminary measurement system is developed in Aalborg University, Denmark to validate the proposed calibration procedure. The objective is to validate how well the proposed calibration procedure works in practical setups using vector network analyzer (VNA).

A. Measurement Setup

The schematic and photo of the measurement system are illustrated in Fig 6 and Fig. 7, respectively, which is composed of:

- A VNA;
- Two programmable attenuators (connected with two probe antennas) with a resolution of 1 dB and covering a range up to 100 dB.
- Two digital phase shifters (connected with two probe antennas) with a step-size of 1^o and covering a 360^o range.
- One 1-to-2 power splitter connected with the probe antennas.
- Two DUT antennas and two probes antennas selected from two identical uniform linear arrays, each of which contains 16 modified vertical polarized Vivaldi antennas with a gain of 9 dBi at 2.7 GHz and with an element spacing of 20 cm; the DUT and probe antennas are aligned and set face-to-face with a measurement distance of 12.5 cm.
- A computer controlling the phase shifters and communicating with VNA to save the data.

It should be noted that the phase shifters are not ideal in practice, where an amplitude uncertainty within ± 0.1 dB and a phase uncertainty within $\pm 0.5^o$ might be introduced for each phase state according to the data sheet. A similar uncertainty in amplitude and phase might be introduced by the attenuators for each attenuator state as well.

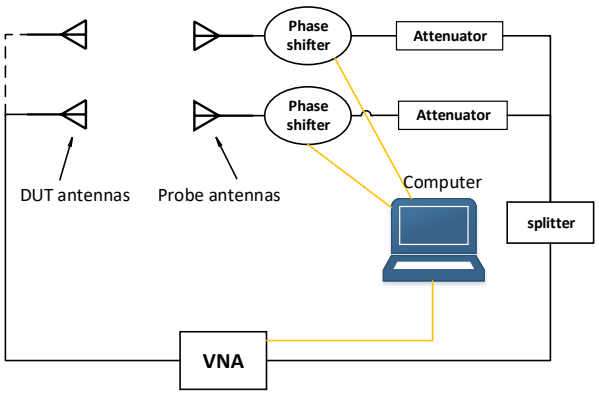

Figure 6. Schematic of the measurement system.

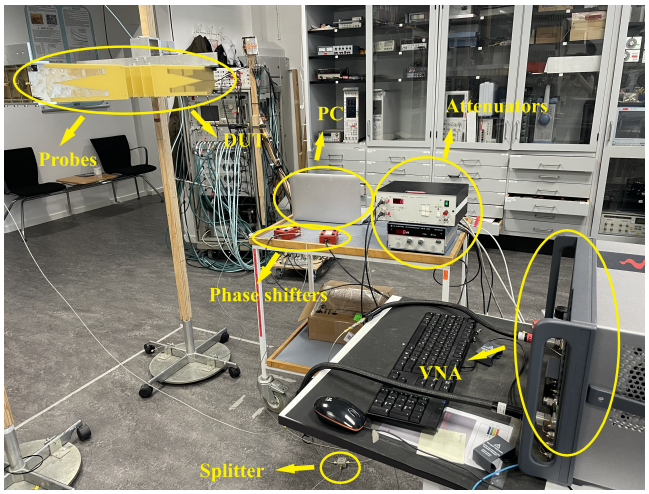

Figure 7. Photo of the measurement system.

B. Measurement procedure

With the proposed calibration method, both probe antennas are connected to the splitter, meaning that the probe antennas radiate simultaneously. According to the calibration procedure presented in section III-A, 3 sets of measurements were conducted as detailed below:

- Fix the attenuator to 0 dB and the phase shifter to 0^o for the 1st probe antenna, and fix the attenuator to 0 dB and rotate the phase shifter from 0^o to 360^o with a step-size of 1^o for the 2nd probe antenna. For each phase state, we record the power values at the DUT antenna ports, i.e. $P_1^1(\phi)$ and $P_1^2(\phi)$, respectively. The maximal RSRP $P_1(\phi)$ is obtained via selecting the larger one, i.e. $P_1(\phi) = \max\{P_1^1(\phi), P_1^2(\phi)\}$.
- Keep the setting as in the first set of measurement except fixing the attenuator to -6 dB for the 1st probe antenna and redo the measurement. The maximal RSRP $P_2(\phi) = \max\{P_2^1(\phi), P_2^2(\phi)\}$ is obtained.
- Keep the setting as in the first set of measurement except fixing the attenuator to -6 dB for the 2nd probe antenna and redo the measurement. The maximal RSRP $P_3(\phi) = \max\{P_3^1(\phi), P_3^2(\phi)\}$ is obtained.

Note that RSRPs at both DUT antenna ports were recorded in

3 sets of measurements for validation purpose. As discussed in section III, RSRPs at both DUT antenna ports should be visible in the power curves, implying RSRP levels at both DUT antenna ports should be comparable. Therefore, the scaling factors $\alpha_1 = \alpha_2 = 0.5$, i.e. -6dB, are set in the measurement to adjust the visible segments of the RSRP curves of the DUT antenna ports. The measurement data $[\mathbf{P}_1\ \mathbf{P}_2\ \mathbf{P}_3]$ is illustrated by the black dots in Fig. 9, where $\mathbf{P}_1$, $\mathbf{P}_2$ and $\mathbf{P}_3$ are plotted in the top, middle and bottom sub-figure, respectively. It can be observed that the measured curve sectors (the black dots) between the discontinuous points are not completely smooth as a cosine curve, due to the unavoidable noises in the practical setup as explained in Section II.B.

C. Measurement Results

Once the measurement data $[\mathbf{P}_1\ \mathbf{P}_2\ \mathbf{P}_3]$ are recorded, the PSO algorithm is applied to seek for the transfer function matrix $\mathbf{A}$ that would satisfy the objective function in (6). As discussed, 10 realizations are run to find the global optimization solution. The converging curves with the PSO algorithm for the 10 realizations are plotted in Fig. 8. It can be observed that only 1 realization out of 10 stagnates in a local optimization solution, while the rest 9 realizations converge to the global optimization solution, demonstrating the high likelihood to find the global optimization solution with the proposed PSO algorithm. Based on the results of the 10 realizations, the estimated $\hat{\mathbf{A}}$ with the minimum distance function $F(\mathbf{A})$ is selected as the estimate of the transfer matrix $\mathbf{A}$.

Based on the best estimation of the transfer function matrix, i.e. $\hat{\mathbf{A}}$, the power curves $\mathbf{P}_1$, $\mathbf{P}_2$ and $\mathbf{P}_3$ can be reconstructed according to (3)-(5) via setting $\alpha_1 = \alpha_2 = 0.5$, as shown by the blue plus signs in Fig. 9. Via comparing the measured power curves with the estimated ones, we can see that small deviations between them in each sub-figure, implying that a good estimate of the transfer function matrix $\mathbf{A}$ is obtained with the proposed method.

As mentioned in the measurement procedure, the RSRPs of both DUT antenna ports were recorded for validation purpose. The estimated RSRPs at both DUT antenna ports, which can be calculated based on the estimated transfer function matrix, i.e. $\hat{\mathbf{A}}$, are compared with the respective measured RSRPs, as illustrated in Fig. 10. It presents excellent agreements between the measured and the estimated RSRPs at both DUT antenna ports for 3 different measurement settings, which further demonstrates that the transfer function matrix $\mathbf{A}$ is estimated with a high accuracy via applying the proposed method.

The efficiency of the proposed calibration method can be further validated via comparing the isolation levels before and after calibration. As explained in [15]–[17], the isolation level for the nth wireless cable for a 2×2 MIMO is defined as:

$$\eta_n(\mathbf{W}_n) = \frac{\mathrm{RSRP}_n(\mathbf{W}_n)}{\mathrm{RSRP}_{\tilde{n}}(\mathbf{W}_n)}, n \neq \tilde{n}, \tag{8}$$

where $\mathbf{W}_n \in \mathbb{C}^{K\times N}$ denotes the calibration weight matrix to establish the nth wireless cable connection and $\mathrm{RSRP}_n(\mathbf{W}_n)$ represents the RSRP value recorded at the nth DUT antenna port when weight matrix $\mathbf{W}_n$ is implemented.

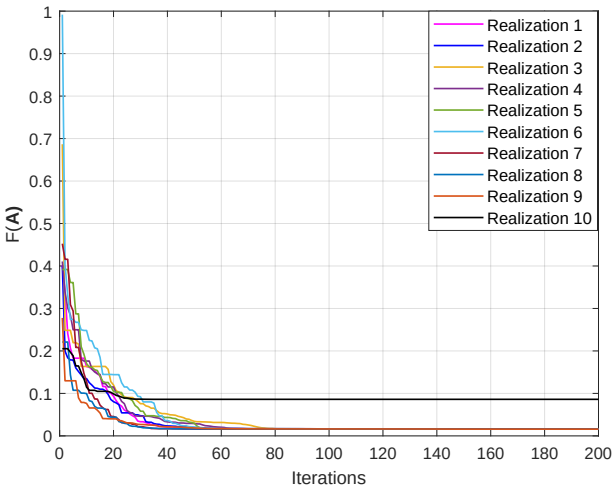

Figure 8. Converging curves of the PSO algorithm for 10 realizations.

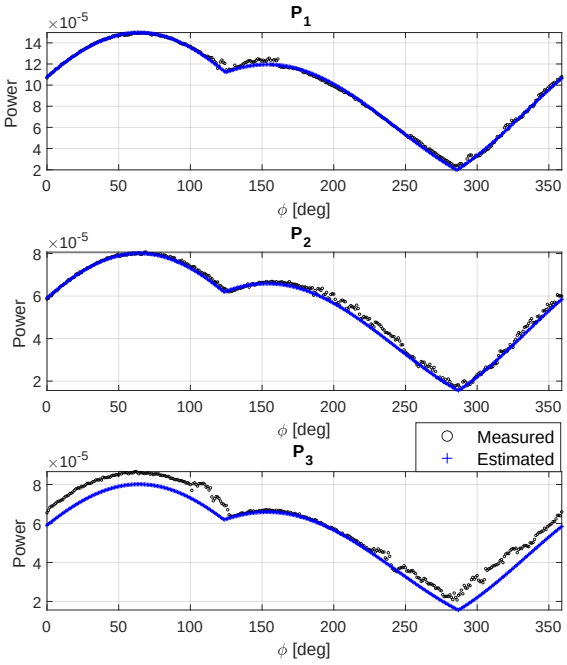

Figure 9. Comparison between the measured and the estimated maximal power vectors with $\mathbf{P}_1$, $\mathbf{P}_2$ and $\mathbf{P}_3$ in the top, middle and bottom sub-figure, respectively.

The isolation levels before calibration are measured via setting $\mathbf{W}_1 = \begin{bmatrix} 1 & 0 \\ 0 & 0 \end{bmatrix}$ and $\mathbf{W}_2 = \begin{bmatrix} 0 & 0 \\ 0 & 1 \end{bmatrix}$, respectively. Consequently, the isolation levels before calibration are simply given by

$$\tilde{\eta}_n(\mathbf{W}_n) = \left| \frac{a_{nn}}{a_{\tilde{n}n}} \right|^2, n \neq \tilde{n}. \tag{9}$$

The above equation indicates that the isolation levels before calibration can be simply obtained via S-parameter measurements between the DUT antenna ports and probe antenna

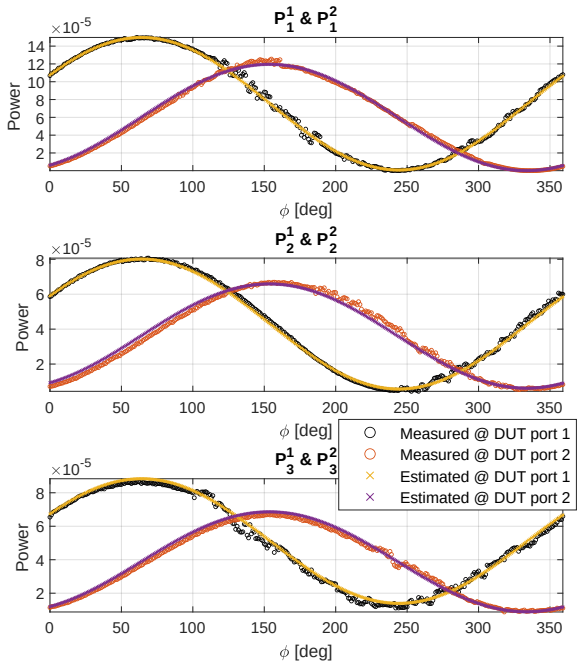

Figure 10. Comparison between the measured and the estimated RSRP vector per DUT port with $\mathbf{P}_1^1$ and $\mathbf{P}_1^2$ in the top sub-figure, $\mathbf{P}_2^1$ and $\mathbf{P}_2^2$ in the middle sub-figure, and $\mathbf{P}_3^1$ and $\mathbf{P}_3^2$ in the bottom sub-figure.

ports.

To measure the isolation levels after calibration, the RSRPs at both DUT antenna ports are measured when the calibration weight matrix $\mathbf{W}_n$ is implemented with the help of the attenuators and the phase shifters. More specifically, to validate the isolation level of the nth wireless cable connection, the RSRPs at both DUT antenna ports are measured via implementing the calibration weight matrix $\mathbf{W}_n$, whose n-th column vector is set to the n-th column vector of $\hat{\mathbf{A}}^{-1}$ and rest entries are set to 0. The isolation level η_n is calculated via substituting the measured RSRP values into (8). The measured isolation levels before and after calibration are compared in Table I. It shows that the isolation levels are low before calibration. That is, strong cross-talk signals (which might even be stronger than the desired signals) appear at both DUT antenna ports. This is due to the fact that the measurement distance between the probe antenna and the DUT antenna is small and strong coupling exists among the antennas. In contrast, the isolation levels of 25.8 dB and 26 dB are achieved for 1st and 2nd wireless cable connections with the proposed wireless cable solution, respectively, indicating good wireless cable connections are established. Therefore, the testing signals with negligible distortion arrives at DUT antenna ports, after calibration. It is worth noting that the non-idealities of the system, e.g. quantization errors and uncertainties of the attenuators and the phase shifters, are involved in the measurement, validating the efficiency and robustness of the proposed wireless cable method in practical measurement systems.

V. Conclusion

The wireless cable solution has been considered as a promising candidate to replace the conducted cable testing method, due to its capability of achieving the equivalent functionality of the conducted cable testing without the need of actual cable connections. In this paper, a novel wireless cable method is proposed to establish the wireless cable connections only relying on the maximal RSRP measurement among DUT antenna ports, instead of RSRP measurements at all DUT ports. Comparing to the state-of-art methods, which require RSRP measurement of each individual DUT antenna port, the proposed method requires less information reported by the DUT, i.e. only the maximal RSRP measurement selected from RSRP measurements of DUT antenna ports. The principle of the proposed method is firstly explained with the detailed derivations. The efficiency of the method is further validated by the experimental measurements, where the non-idealities of a practical system, e.g. quantization error and uncertainties of attenuators and phase shifters, and noise in the measurement, are considered as well. An excellent isolation of above 25 dB is achieved for the 2×2 MIMO system in the validation measurement.

Table I
Isolation level comparison.

	η_1 [dB]	η_2 [dB]
Before calibration	1.5	-0.8
After calibration	25.8	26.0

There are some logic extension of current work. The discussion and validation in this work is limited to 2×2 MIMO radios. It would be desired that the solution can be generalized for MIMO terminals with arbitrary order. VNA measurement system is employed to validate the principle of the proposed algorithm in the work. It is of interest to implement the algorithm with commercial radio communication tester, commercial CE and mobile terminals, and validate it in actual throughput measurement. In this work, the PSO algorithm is applied to determine the transfer matrix $\mathbf{A}$. Though highly effective, it is of interest to see whether closed-form solution can be found to speed up the calibration time in the measurement.

References

[1] M. Rumney, "Testing 5g: Time to throw away the cables," *Microw. J.*, vol. 59, no. 11, 2016.

[2] W. Fan, P. Kyosti, M. Rumney, X. Chen, and G. F. Pedersen, "Over-the-air radiated testing of millimeter-wave beam-steerable devices in a cost-effective measurement setup," *IEEE Communications Magazine*, vol. 56, no. 7, pp. 64–71, 2018.

[3] M. Lorenz, W. Kotterman, and G. Del Galdo, "On modeling ota channel emulation systems," 2018.

[4] M. Gustafsson, T. Jämsä, and M. Högberg, "Ota methods for 5g bts testing—survey of potential approaches," in *2017 XXXIInd General Assembly and Scientific Symposium of the International Union of Radio Science (URSI GASS)*. IEEE, 2017, pp. 1–4.

[5] Y. Qi, G. Yang, L. Liu, J. Fan, A. Orlandi, H. Kong, W. Yu, and Z. Yang, "5g over-the-air measurement challenges: Overview," *IEEE Transactions on Electromagnetic Compatibility*, vol. 59, no. 6, pp. 1661–1670, 2017.

[6] W. Xue, F. Li, and X. Chen, "Effects of signal bandwidth on total isotropic sensitivity measurements in reverberation chamber," *IEEE Transactions on Instrumentation and Measurement*, vol. 70, pp. 1–8, 2021.

[7] Y. Li, L. Xin, X. Liu, and X. Zhang, "Dual anechoic chamber setup for over-the-air radiated testing of 5g devices," *IEEE Transactions on Antennas and Propagation*, vol. 68, no. 3, pp. 2469–2474, 2019.

[8] X. Chen, W. Fan, L. Hentilä, P. Kyösti, and G. F. Pedersen, "Throughput modeling and validations for mimo-ota testing with arbitrary multipath," *IEEE Antennas and Wireless Propagation Letters*, vol. 17, no. 4, pp. 637–640, 2018.

[9] M. G. Nilsson, P. Hallbjörner, N. Arabäck, B. Bergqvist, T. Abbas, and F. Tufvesson, "Measurement uncertainty, channel simulation, and disturbance characterization of an over-the-air multiprobe setup for cars at 5.9 ghz," *IEEE Transactions on Industrial Electronics*, vol. 62, no. 12, pp. 7859–7869, 2015.

[10] C. S. P. Lötbäck, K. Karlsson, M. S. Kildal, A. Haliti, M. Nilsson, and R. Iustin, "Evaluation of complete vehicle over-the-air verification methods for multiple-input multiple-output communication systems," in *2021 15th European Conference on Antennas and Propagation (EuCAP)*. IEEE, 2021, pp. 1–5.

[11] T. Eichler, U. Philipp, H. Mellein, and L. Rädler, "Virtual cable calibration for ota testing of 5g mmwave devices." *Microwave Journal*, vol. 64, no. 5, 2021.

[12] P. Kyosti and J. Kyrolainen, "Systems and methods for radio channel emulation of a multiple input multiple output (mimo) wireless link," Mar. 24 2020, uS Patent 10,601,695.

[13] J. Kyrolainen and P. Kyosti, "Systems and methods for performing multiple input, multiple output (mimo) over-the-air testing," Jul. 24 2018, uS Patent 10,033,473.

[14] C. Schirmer, M. Lorenz, A. T. Wim, R. Perthold, M. H. Landmann, G. Del Galdo *et al.*, "Mimo over-the-air testing for electrically large objects in non-anechoic environments," in *2016 10th European Conference on Antennas and Propagation (EuCAP)*. IEEE, 2016, pp. 1–6.

[15] W. Fan, P. Kyösti, L. Hentilä, and G. F. Pedersen, "Mimo terminal performance evaluation with a novel wireless cable method," *IEEE Transactions on Antennas and Propagation*, vol. 65, no. 9, pp. 4803–4814, 2017.

[16] W. Fan, F. Zhang, P. Kyösti, L. Hentilä, and G. F. Pedersen, "Wireless cable method for high-order mimo terminals based on particle swarm optimization algorithm," *IEEE Transactions on Antennas and Propagation*, vol. 66, no. 10, pp. 5536–5545, 2018.

[17] F. Zhang, W. Fan, and Z. Wang, "Achieving wireless cable testing of high-order mimo devices with a novel closed-form calibration method," *IEEE Transactions on Antennas and Propagation*, vol. 69, no. 1, pp. 478–487, 2020.

[18] 3GPP TR 36.978 V13.1.0, "Evolved Universal Terrestrial Radio Access (E-UTRA) User Equipment (UE) antenna test function definition for two-stage Multiple Input Multiple Output (MIMO) Over The Air (OTA) test method," 2015.

[19] H. Gao, W. Wang, W. Fan, Y. Wu, Y. Liu, and G. F. Pedersen, "Over-the-air testing for carrier aggregation enabled mimo terminals using radiated two-stage method," *Ieee Access*, vol. 6, pp. 71 622–71 631, 2018.

[20] M. Rumney, H. Kong, Y. Jing, Z. Zhang, and P. Shen, "Recent advances in the radiated two-stage mimo ota test method and its value for antenna design optimization," in *2016 10th European Conference on Antennas and Propagation (EuCAP)*. IEEE, 2016, pp. 1–5.

[21] P. Shen, Y. Qi, W. Yu, J. L. Drewniak, M. Yu, and F. Li, "An rts-based near-field mimo measurement solution—a step toward 5g," *IEEE Transactions on Microwave Theory and Techniques*, vol. 67, no. 7, pp. 2884–2893, 2019.

[22] P. Shen, Y. Qi, W. Yu, J. Fan, Z. Yang, and S. Wu, "A decomposition method for mimo ota performance evaluation," *IEEE Transactions on Vehicular Technology*, vol. 67, no. 9, pp. 8184–8191, 2018.

[23] W. Fan, P. Kyosti, Y. Jing, and Z. Wang, "Over-the-air testing metrology of 5g radios," in *Metrology for 5G and Emerging Wireless Technologies*. Institution of Engineering and Technology, 2021.

[24] 3GPP TS 38.215 V16.4.0, "3rd Generation Partnership Project; Technical Specification Group Radio Access Network; NR; Physical layer measurements'," 2020.

[25] J. Robinson and Y. Rahmat-Samii, "Particle swarm optimization in electromagnetics," *IEEE transactions on antennas and propagation*, vol. 52, no. 2, pp. 397–407, 2004.

[26] M. Clerc, *Particle swarm optimization*. John Wiley & Sons, 2010, vol. 93.

[27] J. Kennedy and R. Eberhart, "Particle swarm optimization," in *Proceedings of ICNN'95-international conference on neural networks*, vol. 4. IEEE, 1995, pp. 1942–1948.

[28] M. Clerc and J. Kennedy, "The particle swarm-explosion, stability, and convergence in a multidimensional complex space," *IEEE transactions on Evolutionary Computation*, vol. 6, no. 1, pp. 58–73, 2002.